ELECTRONIC SUPPLEMENTARY INFORMATION

Highly Improved Water Tolerance of Hydrogel Fibers by Carbon Nanotube Sheath for Rotational, Contractile and Elongational Actuation

Chengwei You,‡[ab] Wenjing Qin,‡[a] Zhe Yan,‡[ab] Zhixin Ren,[ab] Jiayi Huang,[b] Jiatian Ii,[b] Wang Chang,[b]Wenqian He,[b] Kai Wen,[bcd] Shougen Yin,*[a] Xiang Zhou*[bcd] and Zunfeng Liu*[b]

[a]School of Materials Science and Engineering, Key Laboratory of Display Materials and Photoelectric Devices, Tianjin University of Technology, Tianjin, 300384, China.

[b]Key Laboratory of Functional Polymer Materials, College of Chemistry, State Key Laboratory of Medicinal Chemical Biology, Nankai University, Tianjin 300071, China.

[c]School of Chemical Engineering, University of Science and Technology Liaoning, Anshan, 114051, China.

[d]Department of Science, China Pharmaceutical University, Nanjing, Jiangsu, 211198, China.

‡ These authors contributed equally to this work.
* Corresponding authors E-mail: liuzunfeng@nankai.edu.cn (Z.L.), zhouxiang@cpu.edu.cn (X.Z.), sgyin@tjut.edu.cn (S.Y.)

This file contains:

Other supplementary materials for this manuscript include the following:

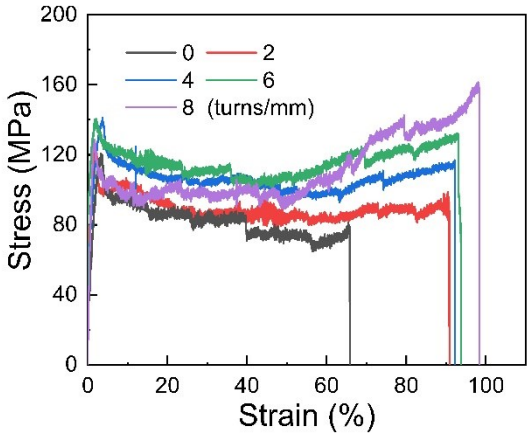

Fig. S1. The stress-strain curves for the hydrogel fiber with different twist density. The strain rate is 5 mm/s. The humidity is 20%.

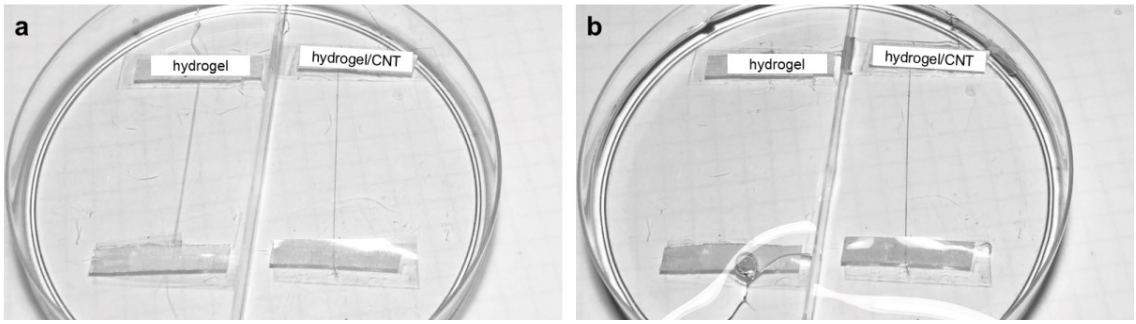

Fig. S2. A hydrogel fiber and A HF-ACNS$_{0°}$ fiber before and after soaking in water with both-end tethered. The hydrogel fiber broke due to supercontraction, and the HF-ACNS$_{0°}$ fiber did not break due to surface coating of carbon nanotube sheets.

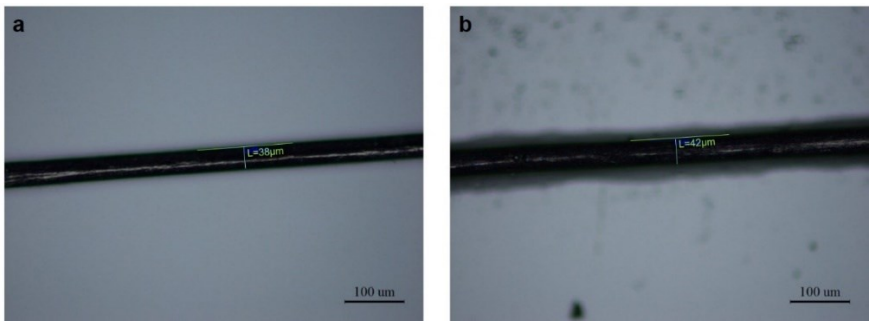

Fig. S3. Optical microscope images for the HF-ACNS$_{0°}$ fiber immersed in water for 15 hours. The diameter of the HF-ACNS$_{0°}$ fiber is (a) 38 μm and (b) 42 μm.

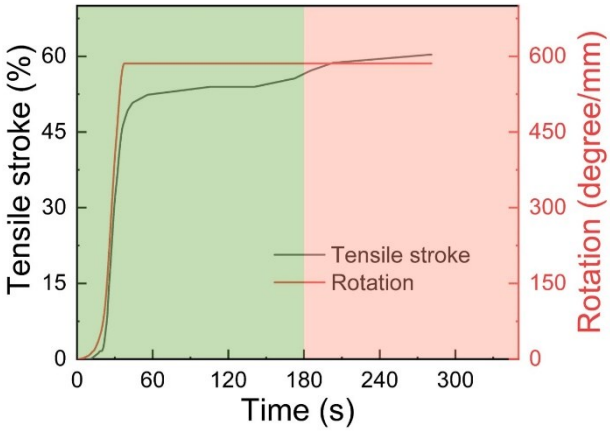

Fig. S4. Tensile stroke and rotation angle as a function of time for two-ply self-balanced hydrogel fibers during an actuation cycle driven by water fog. The twist density was 8 turns mm^{-1}, the diameter of the hydrogel fiber was 50 μm, and the water fog flux was 28.8 g s^{-1}.

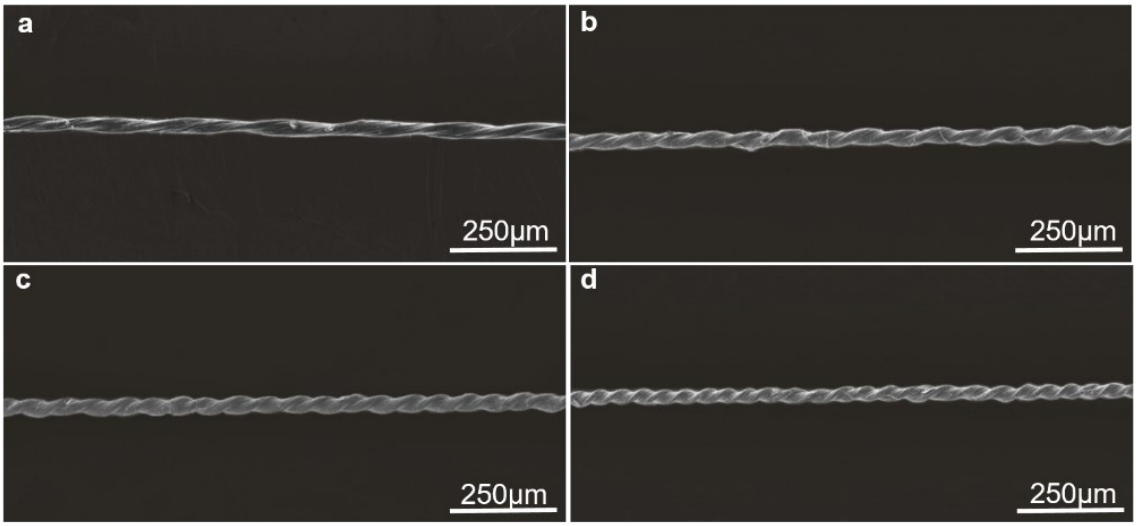

Fig. S5. SEM images for the HF-$ACNS_{0°}$ fibers with different twist densities. For a) to d), the twist densities are 2, 4, 6, and 8 turns mm^{-1}, respectively.

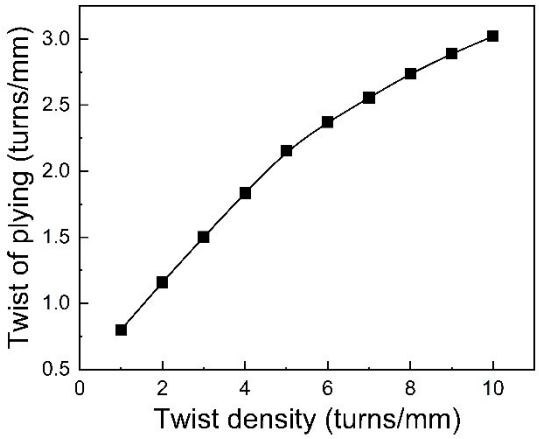

Fig. S6. Twist of plying as a function of inserted twist for a HF-ACNS$_{0^\circ}$ fiber after twist insertion and folding in the middle point.

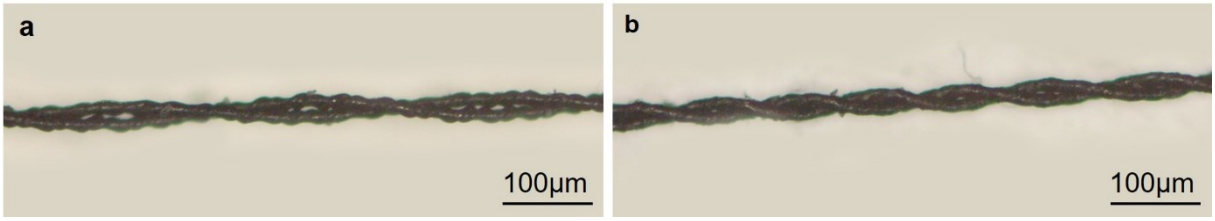

Fig. S7. Optical microscope images for the HF-ACNS$_{0^\circ}$ muscle before and after exposure to ultrasonically-generated water fog. The twist density was 8 turns mm^{-1}, the diameter of the hydrogel fiber was 25 μm, the isobaric load was 0.61 MPa, and the water fog flux was 28.8 g s^{-1}.

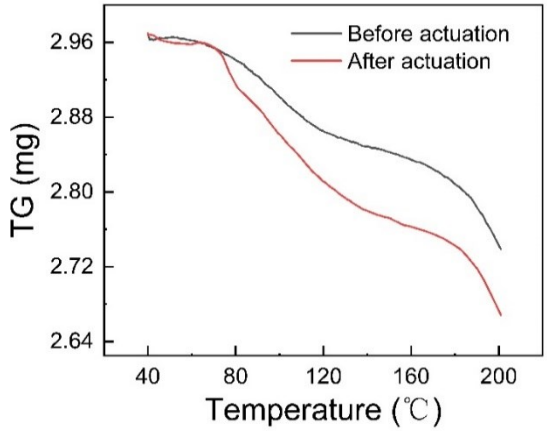

Fig. S8. Thermal gravimetric analysis in N_2 atmosphere for the HF-ACNS$_{0^\circ}$ muscle before and after one cycle of actuation.

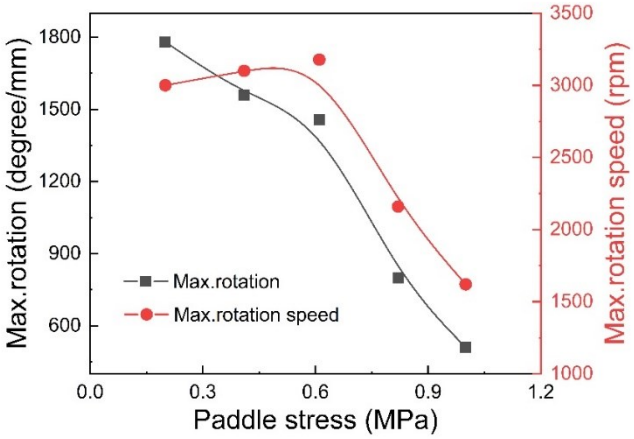

Fig. S9. Maximum rotation angle and maximum rotational speed as a function of isobaric load for the HF-ACNS$_{0°}$ muscle on exposure to ultrasonically-generated water fog. The twist density was 8 turns mm^{-1}, the diameter of the hydrogel fiber was 25 μm, and the water fog flux was 28.8 g s^{-1}.

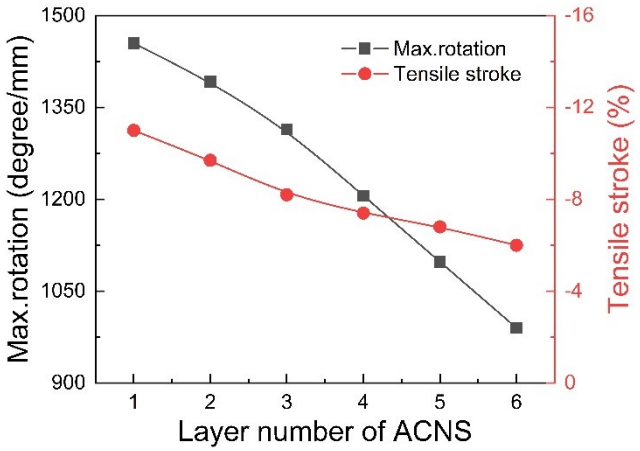

Fig. S10. Maximum rotation angle and maximum tensile stroke as a function of number of layers of ACNS for the HF-ACNS$_{0°}$ muscle on exposure to ultrasonically-generated water fog. The twist density was 8 turns mm^{-1}, the diameter of the hydrogel fiber was 25 μm, and the water fog flux was 28.8 g s^{-1}.

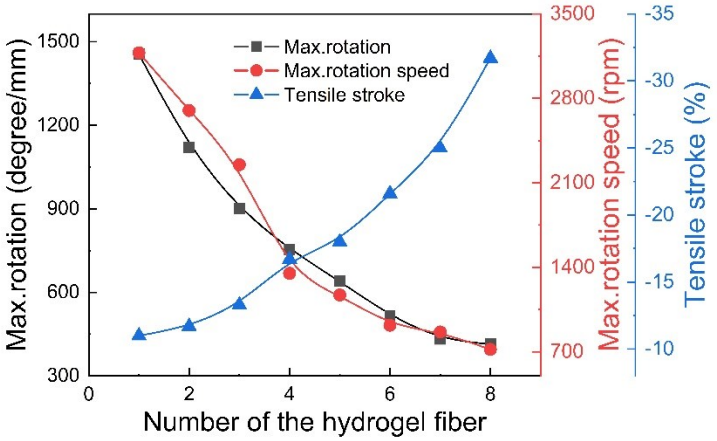

Fig. S11. Maximum rotation angle, maximum rotational speed and tensile stroke as a function of number of the hydrogel fibers used for preparing the HF-ACNS$_{0°}$ muscle on exposure to ultrasonically-generated water fog. The twist density was 8 turns mm^{-1}, the diameter of the hydrogel fiber was 25 μm, and the water fog flux was 28.8 g s^{-1}.

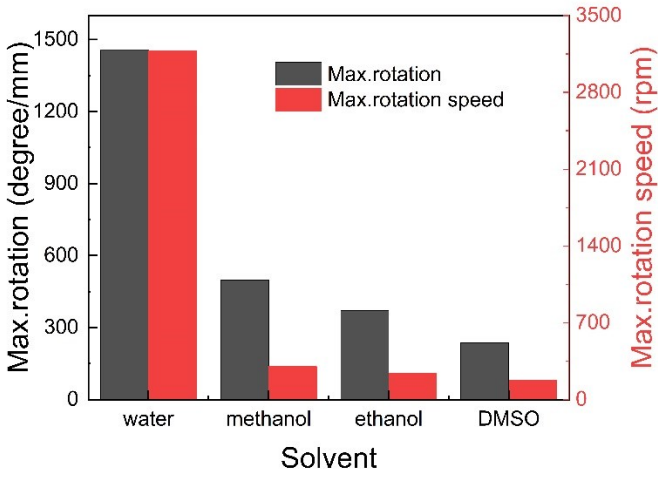

Fig. S12. Maximum rotation angle and maximum rotational speed for the HF-ACNS$_{0°}$ muscle on exposure to different ultrasonically-generated vapors including water, methanol, ethanol, and dimethyl sulfoxide. The twist density was 8 turns mm^{-1}, the diameter of the hydrogel fiber was 25 μm, and the same power was used to generate the fog as water (28.8 g s^{-1}).

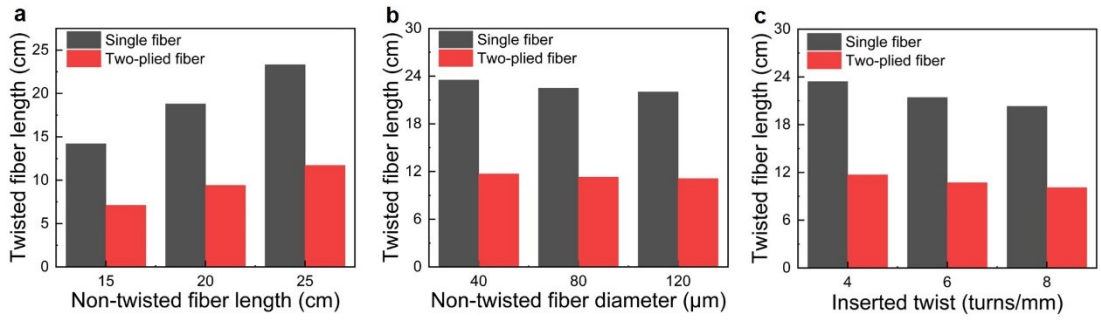

Fig. S13. The length of the plied yarn as a function of the individual fiber length (a), the individual fiber diameter (b), and inserted twist. The fiber twist density in (a) and (b) was 4 turns/mm, the fiber length in (b) and (c) was 25 cm, and the fiber diameter of (a) and (c) was 30 μm.

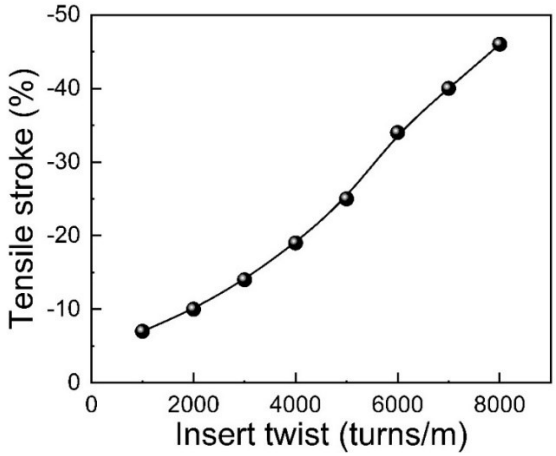

Fig. S14. Maximum tensile stroke as a function of different inserted twist for the HF-ACNS$_{0°}$ muscle on exposure to ultrasonically-generated water fog with the paddle torsionally tethered. The diameter of the hydrogel fiber was 25 μm, the isobaric load of the muscle was 0.61 MPa, and the water fog flux was 28.8 g s^{-1}.

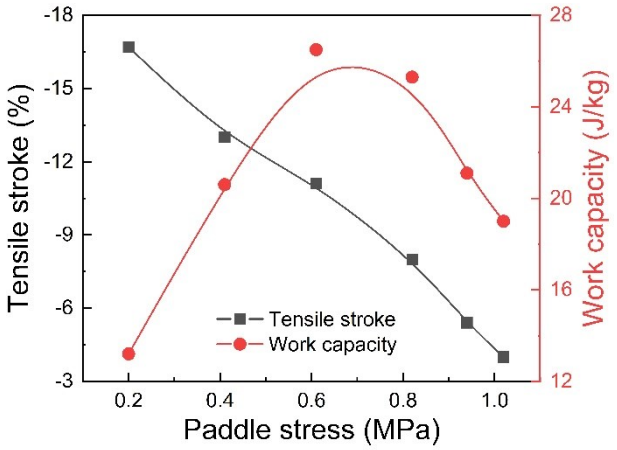

Fig. S15. Maximum tensile stroke and work capacity as a function of isobaric load for the HF-$ACNS_{0°}$ muscle on exposure to ultrasonically-generated water fog. The twist density was 8 turns mm^{-1}, the diameter of the hydrogel fiber was 25 μm, and the water fog flux was 28.8 g s^{-1}. The paddle was torsionally tethered.

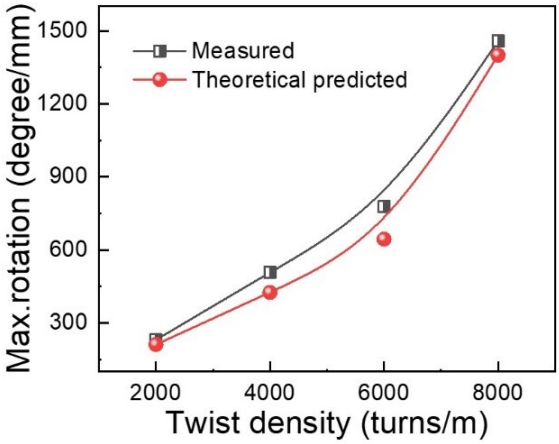

Fig. S16. Measured and theoretically predicted maximum rotation angle as a function of different inserted twist for the HF-$ACNS_{0°}$ muscle on exposure to ultrasonically-generated water fog. The diameter of the hydrogel fiber was 25 μm, the isobaric load of the muscle was 0.61 MPa, and the water fog flux was 28.8 g s^{-1}.

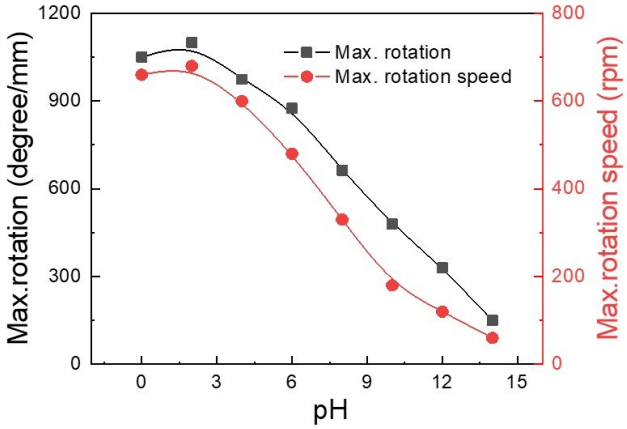

Fig. S17. Maximum rotation angle and maximum rotational speed for the HF-ACNS$_{90°}$ muscle on exposure to ultrasonically-generated water fog as a function of pH. The twist density was 8 turns mm^{-1}, the diameter of the hydrogel fiber was 25 μm, and the water fog flux was 28.8 g s^{-1}.

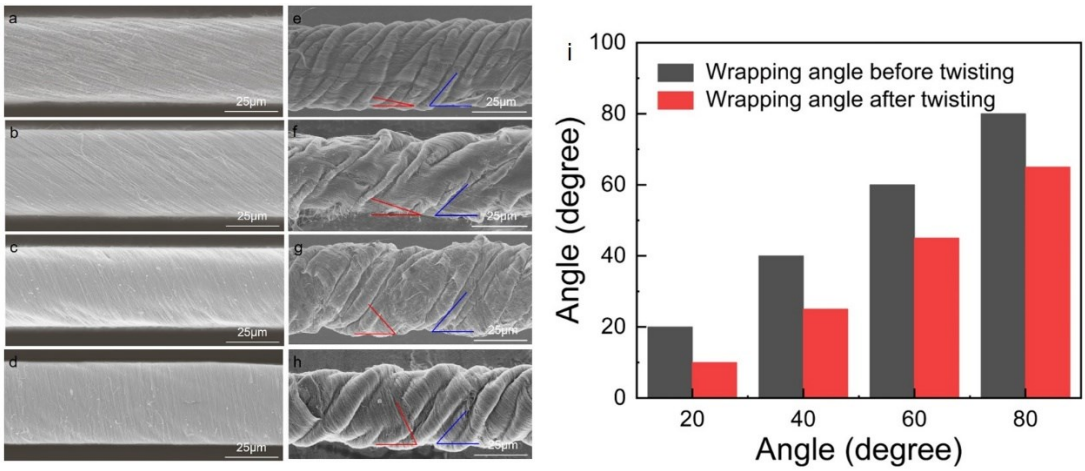

Fig. S18. (a-h) SEM images and (i) bias angle for the (a-d) non-twisted and (e-h) twisted HF-ACNS$_{20°\text{-}80°}$ fibers with different wrapping angles.

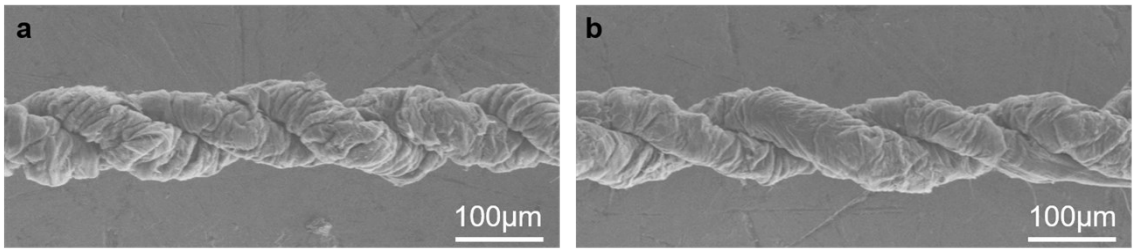

Fig. S19. SEM images for the HF-ACNS$_{90°}$ muscles before and after exposure to ultrasonically-generated water fog. The twist density was 8 turns mm^{-1}, the diameter of the hydrogel fiber was 25 μm, and the water fog flux was 28.8 g s^{-1}.

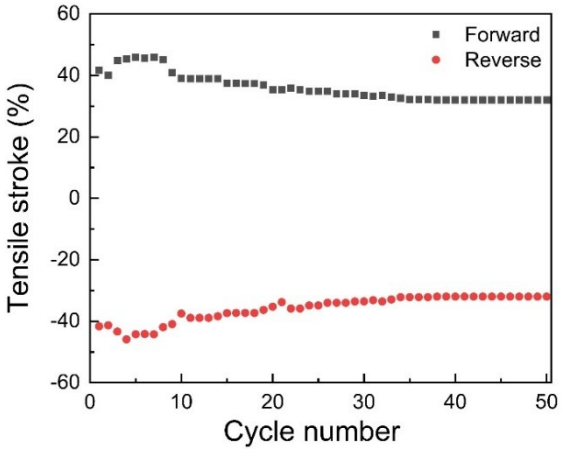

Fig. S20. Maximum tensile stroke as a function of cycle number for the HF-ACNS$_{90°}$ muscle on exposure to ultrasonically-generated water fog. The twist density was 8 turns mm^{-1}, the diameter of the hydrogel fiber was 25 μm, and the water fog flux was 28.8 g s^{-1}.

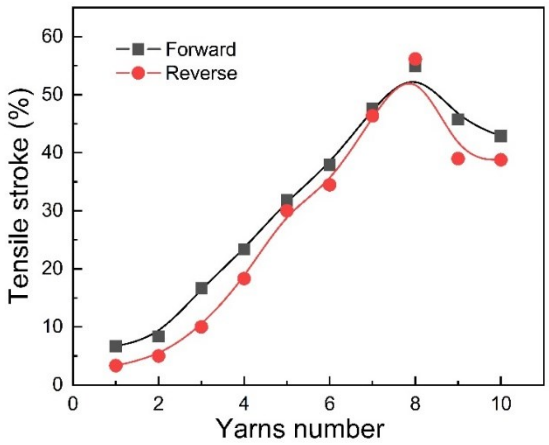

Fig. S21. Maximum strain as a function of number of the hydrogel fiber used for preparing the HF-ACNS$_{90°}$ muscle on exposure to ultrasonically-generated water fog. The twist density was 8 turns mm^{-1}, the diameter of the hydrogel fiber was 25 μm, and the water fog flux was 28.8 g s^{-1}.

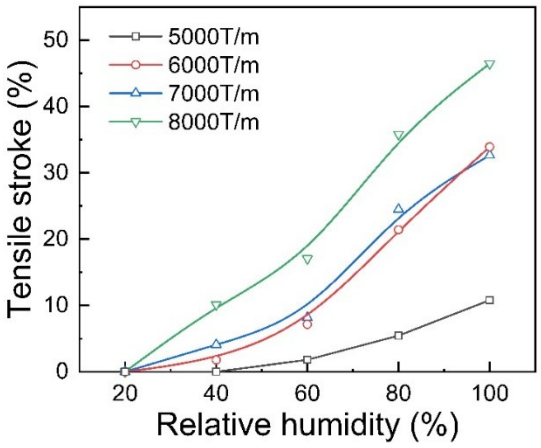

Fig. S22. Maximum tensile stroke as a function of relative humidity for the HF-ACNS$_{90°}$ muscles with different inserted twist, with the paddle torsionally tethered. The diameter of the hydrogel fiber was 25 μm, and the isobaric load of the muscle was 0.61 MPa.

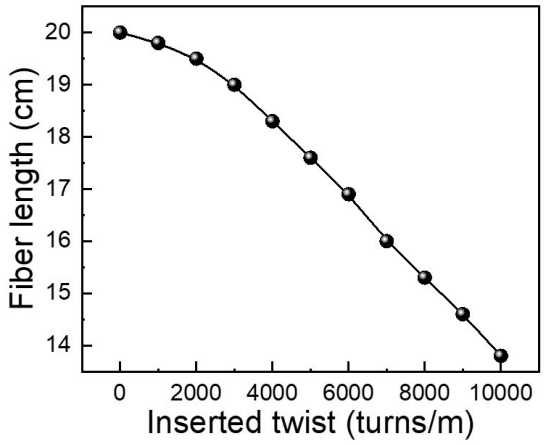

Fig. S23. Fiber length as a function of inserted twist for the HF-ACNS$_{0°}$ fibers. The diameter of the HF-ACNS$_{0°}$ fiber was 25 μm, the relative humidity was 20%.

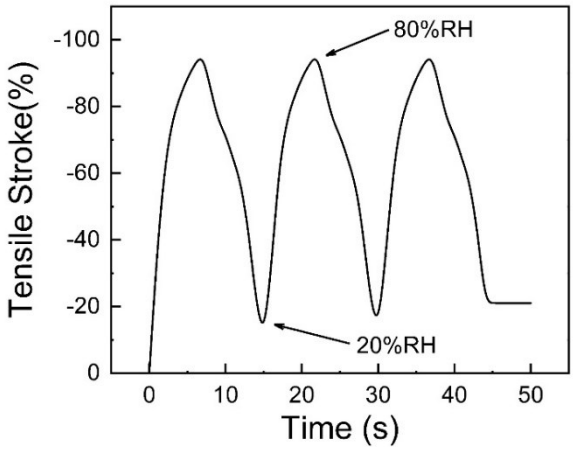

Fig. S24. Tensile actuation stroke as a function of time for a homochiral (ZZ) HF-ACNS$_{0°}$ coil on exposure to relative humidity of 80%. The twist density was 6 turns mm^{-1}, the diameter of the hydrogel fiber was 25 μm, the spring index was 15, the coil pitch was 1 mm, and the relative humidity was 80%. The coil muscle was non-loaded.

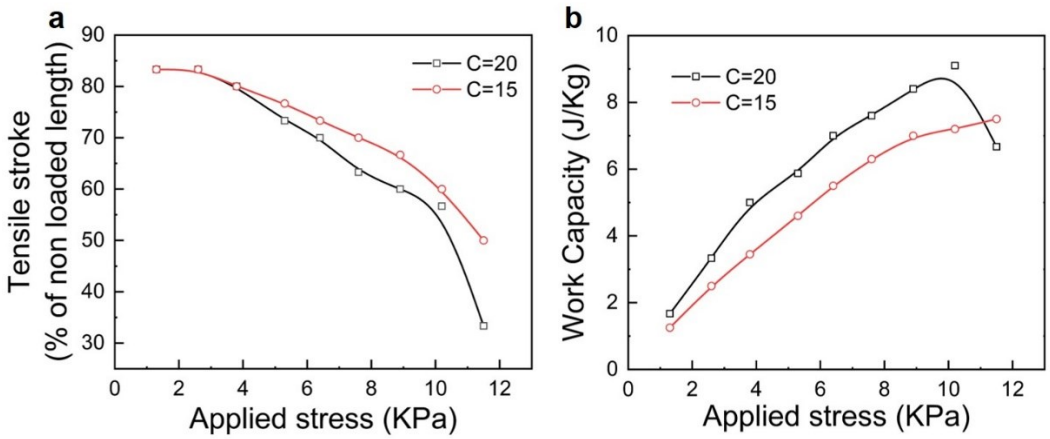

Fig. S25. (a) Tensile actuation stroke and (b) work capacity as a function of applied stress for homochiral HF-ACNS$_{0°}$ coils with different spring index on exposure to ultrasonically-generated water fog. The twist density was 6 turns mm^{-1}, the diameter of the hydrogel fiber was 25 μm, the coil pitch was 1 mm, and the relative humidity was 80%.

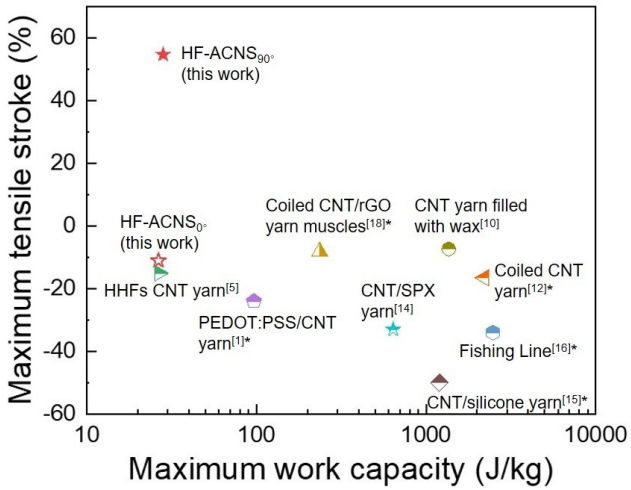

Fig. S26. Comparison of the tensile actuation performance of HF-ACNS$_x$ muscles in this paper with typical fiber artificial muscles reported in literatures. The detailed data are shown in Table S2.

Table S1. Comparison of the torsional actuation performance of HF-ACNS$_x$ muscles in this paper with typical fiber artificial muscles reported in literatures.

Material	Stimulation	Torsional rotate (degree·mm^{-1})	Normalized torsional rotate (degree·μm mm^{-1})	Torsional speed (rpm)	fractional rotation (degree/turns mm^{-1})
HF-ACNS$_{0°}$ muscle (this work)	water	1455	51434	3178	9712
HF-ACNS$_{90°}$ muscle (this work)	water	501	35442	720	5198
PEDOT:PSS/CNT yarn[1]	water	1340	40200	1395	3453
Oxygen plasma treated CNT yarn [2]	water	61.3	2452	750	—
Twisted Graphene hydrogel fiber [3]	water	588	38220	5190	23250
Silkworm silk muscle [4]	water	547	14696	1125	6078
HHFs CNT yarn [5]	alcohol	738	47970	6361	—
CNT yarn treated with ITAP [6]	acetone	52	5200	160	58.4
CNT Yarn deposited with HC–BA NG [7]	glucose	40	1200	<0.5	1429
CNT yarn filled with wax and SEBS [8]	electro-thermal	80	1500	9800	1404
CNT yarn filled with PVA/H_2SO_4[9]	electricity	53	1537	2330	18.7
CNT yarn filled with wax [10]	electro-thermal	17.4	174	11500	54.6
CNT yarn [11]	electricity	125	1500	590	674

HHFs: hierarchically arranged helical fibers; ITAP: incandescent tension annealing process; HC–BA NG: boronic acid-conjugated hyaluronic acid/cholesterol nanogel; SEBS: polystyrene-poly(ethylene–butylene)-polystyrene; PVA: polyvinyl alcohol.

Table S2. Comparison of the tensile actuation performance of HF-ACNS$_x$ muscles in this paper with typical fiber artificial muscles reported in literatures.

Material	Diameter (μm)	Maximum tensile stroke (%)	Torsionally tethered	Maximum work capacity (J kg^{-1})
HF-ACNS$_{0°}$ muscle (this work)	25	-11 / -46	no / yes	26.5
HF-ACNS$_{90°}$ muscle (this work)	70	54.8 / 52	no / yes	28.2
PEDOT:PSS/CNT yarn [1]	30	-24* / -68*	no / yes	96.9
Twisted Graphene hydrogel fiber [2]	62	4.7	no	—
Silkworm silk [4]	82	-70*	no	73
HHFs CNT yarn [5]	65	-15 / -59*	no	—
CNT yarn filled with wax [10]	115	-7.3	no	1360
CNT yarn [11]	12	-1	no	—
Coiled CNT yarn [12]	300	-16.5*	no	2200
CNT yarn filled with PDDA [13]	67	-78*	no	2170
CNT/SPX yarn [14]	—	-33	no	640
CNT/silicone yarn [15]	500	-50*	no	1200
Fishing Line [16]	127	-34*	no	2480
Coiled GO/Nylon fiber [17]	76	-80* / 75*	no	—
Coiled CNT/rGO yarn muscles [18]	58	-8.1*	no	236

*The samples were coiled or self-coiled.

GO: graphene oxide; PDDA: poly(diallyldimethylammonium chloride); SPX spandex; rGO: reduced graphene oxide.

Movie captions:

Movie S1. Comparison of water resistance properties of pure hydrogel fiber and the HF-$ACNS_{0°}$ fiber. On the left side of the culture dish is a 50-μm-diameter hydrogel fiber, and on the right side of the culture dish is a HF-$ACNS_{0°}$ fiber. The hydrogel fiber broke upon immersion in water, while the HF-$ACNS_{0°}$ fiber did not break in water. The HF-$ACNS_{0°}$ fiber were prepared by coating one layer of CNT sheet (sheet width of 0.5 cm) on a 50-μm hydrogel fiber.

Movie S2. Hygromorph torsional and contractile actuation of the twisted, two ply HF-$ACNS_{0°}$ fiber, which was driven by water fog. The twist density was 8 turns mm^{-1}, the diameter of the hydrogel fiber was 25 μm, and the water fog flux was 28.8 g s^{-1}.

Movie S3. Hygromorph torsional and elongational actuation of the twisted HF-$ACNS_{90°}$ fibers that was assembled from 8 plies of 25-μm-diameter hydrogel fiber with water fog. The twist density was 8 turns mm^{-1}, and the water fog flux was 28.8 g s^{-1}.

References

1 X. Gu, Q. Fan, F. Yang, L. Cai, N. Zhang, W. Zhou, W. Zhou and S. Xie, *Nanoscale*, 2016, **8**, 17881-17886.

2 S. He, P. Chen, L. Qiu, B. Wang, X. Sun, Y. Xu and H. Peng, *Angew. Chem.*, 2015, **127**, 15093-15097.

3 H. Cheng, Y. Hu, F. Zhao, Z. Dong, Y. Wang, N. Chen, Z. Zhang and L. Qu, *Adv. Mater.*, 2014, **26**, 2909-2913.

4 T. Jia, Y. Wang, Y. Dou, Y. Li, M. Jung de Andrade, R. Wang, S. Fang, J. Li, Z. Yu, R. Qiao, Z. Liu, Y. Cheng, Y. Su, M. Minary-Jolandan, R. H. Baughman, D. Qian and Z. Liu, *Adv. Funct. Mater.*, 2019, **29**, 1808241.

5 P. Chen, Y. Xu, S. He, X. Sun, S. Pan, J. Deng, D. Chen and H. Peng, *Nat. Nanotechnol.*, 2015, **10**, 1077-1083.

6 J. Di, S. Fang, F. A. Moura, D. S. Galvao, J. Bykova, A. Aliev, M. J. de Andrade, X. Lepro, N. Li, C. Haines, R. Ovalle-Robles, D. Qian and R. H. Baughman, *Adv. Mater.* 2016, **28**, 6598-6605.

7 J. Lee, S. Ko, C. H. Kwon, M. D. Lima, R. H. Baughman and S. J. Kim, *Small*, 2016, **12**, 2085-2091.

8 K. Y. Chun, S. Hyeong Kim, M. Kyoon Shin, C. Hoon Kwon, J. Park, Y. Tae Kim, G. M. Spinks, M. D. Lima, C. S. Haines, R. H. Baughman and S. Jeong Kim, *Nat. Commun.* 2014, **5**, 3322.

9 J. A. Lee, Y. T. Kim, G. M. Spinks, D. Suh, X. Lepro, M. D. Lima, R. H. Baughman and S. J. Kim, *Nano Lett.* 2014, **14**, 2664-2669.

10 M. D. Lima, N. Li, M. Jung de Andrade, S. Fang, J. Oh, G. M. Spinks, M. E. Kozlov, C. S. Haines, D. Suh, J. Foroughi, S. J. Kim, Y. Chen, T. Ware, M. K. Shin, L. D. Machado, A. F. Fonseca, J. D. Madden, W. E. Voit, D. S. Galvao and R. H. Baughman, *Science*, 2012, **338**, 928-932.

11 J. Foroughi, G. M. Spinks, G. G. Wallace, J. Oh, M. E. Kozlov, S. Fang, T. Mirfakhrai, J. D. Madden, M. K. Shin, S. J. Kim and R. H. Baughman, *Science*, 2011, **334**, 494-497.

12 J. A. Lee, N. Li, C. S. Haines, K. J. Kim, X. Lepro, R. Ovalle-Robles, S. J. Kim and R. H. Baughman, *Adv. Mater.*, 2017, **29**, 1700870.

13 S. H. Kim, C. H. Kwon, K. Park, T. J. Mun, X. Lepro, R. H. Baughman, G. M. Spinks and S. J. Kim, *Sci. Rep.*, 2016, **6**, 23016.

14 J. Foroughi, G. M. Spinks, S. Aziz, A. Mirabedini, A. Jeiranikhameneh, G. G. Wallace, M. E. Kozlov and R. H. Baughman, *ACS Nano*, 2016, **10**, 9129-9135.

15 M. D. Lima, M. W. Hussain, G. M. Spinks, S. Naficy, D. Hagenasr, J. S. Bykova, D. Tolly and R. H. Baughman, *Small* 2015, **11**, 3113-8.

16 C. S. Haines, M. D. Lima, N. Li, G. M. Spinks, J. Foroughi, J. D. W. Madden, S. H. Kim, S. Fang, M. Jung de Andrade, F. Göktepe, Ö. Göktepe, S. M. Mirvakili, S. Naficy, X. Lepró, J. Oh, M. E. Kozlov, S. J. Kim, X. Xu, B. J. Swedlove, G. G. Wallace and R. H. Baughman, *Science*, 2014, **343**, 868-872.

17 H. Kim, J. H. Moon, T. J. Mun, T. G. Park, G. M. Spinks, G. G. Wallace and S. J. Kim, *ACS Appl. Mater. Interfaces,* 2018, **10**, 32760.

18 J. Qiao, J. Di, S. Zhou, K. Jin, S. Zeng, N. Li, S. Fang, Y. Song, M. Li, R. H. Baughman and Q. Li, *Small,* 2018, **14**, 1801883.